Thermophysics and Aeromechanics, *2021*, *Vol. 28*, *No. 1*

DOI: 10.1134/S0869864321010091

Modeling of heat transfer due to induction heating of laminated glass-metal materials*

O.N. Lyubimova and M.A. Barbotko

Far Eastern Federal University, *Vladivostok*, *Russia*

E-mail: barbotko_ma@dvfu.ru

(*Received February 23*, *2020*; *revised June 25*, *2020*;
accepted for publication August 5, *2020*; *further refined October 5*, *2020*)

The heat-induced variations in material properties for a layered glass-metal composite material were studied for the case of induction heating and the subsequent composite annealing of the sample. A cylindrical sample of the composite (outer metal cylinder covering the glass cylinder) was used in our experimental study. This sample is an imitation of a brittle rock under a high stress. The simulation complexity originates from superposition of the glass point transition within the glass layer, induction heating for the whole sample, and heat radiation from the external metallic surface. Structural and mechanical relaxation processes in glass are calculated using the Boltzmann–Volterra superposition and the Tula–Narayanaswami–Mazurin–Moynihan (TNMM) model based on introducing a structural temperature as an additional parameter. The paper offers a mathematical model and a simulation method for calculating the temperature field and material properties distributions during the composite production process. The simulation results are presented for various regimes of heating and for glass-metal composite properties. This approach is useful for evaluating the operation modes of the glass layer annealing and for estimating the evolution of laminated composite materials.

Keywords: induction heating, glass-metal composite, glass phase transition, complex heat transfer in layered materials.

Introduction

Production of many types of engineering materials assumes a high thermal impact that changes the phase state of the ingredients. One of promising innovative materials is glass-and-metal material — the glass-metal composites [1]. The most reliable and economic production method for this material is induction heating [2]. The key factors for using the inductive heating are a high efficiency and a lower output of oxide scale on the metal layer (this reduces the metal loss and improves cohesion to the glass layer). The following processes occur during inductive heating: energy transfer from the induction loop (AC-fed at a certain frequency) to the heated item by electromagnetic field; temperature growth for the item with a given shape from the initial to the top level of temperature; the structural changes occurring during sample heating and after-process cooling (this influences the properties of the final material). The present paper offers a mathematical description for both thermal problems.

* Research was supported by the Russian Foundation for Basic Research through the science project No. 19-33-90200.

The complexity in modeling the process parameters (for glass-metal composite production technology) is due to the glass rheology changes (caused by temperature variation and glass transition process). Although the theory of vitrification (aka glass transition) is supported by numerous theoretical and experimental papers [3–11], the general theoretical approach suitable for detailed description of available experimental data is not available yet. There exist two main approaches for describing the thermal processes and structural changes in vitrifying materials: modeling of vitrification as a phase transition (e.g., [12, 13]) and the kinetic theory of vitrification (see publications [7, 10]). These theoretical models are supported by experimental facts on the glass transition temperature and glass transition boundaries vs. temperature change rate and data on the temperature treatment prehistory. One of the approaches within the kinetic theory has been developed by O.V. Mazurin and co-workers: this is the relaxation theory of vitrification and the method of glass characterization while glass transition phase [3, 4, 6]. This approach was tested over a big volume of experimental data, including the cases of glass-material seal backing [3, 4]. The basics of this method is an idea promoted by A. Tula about improving the model of vitrification within the annealing range by introducing an extra systematic parameter — the "fictitious temperature" T_f [11]. The later publications [4, 8, 9] formulated the main assumptions of the relaxation theory of vitrification and developed the simulation algorithms for glass structural relaxation (for glass of any composition). These algorithms have no big differences, so the researches typically present them together as the Tula–Narayanaswami–Mazurin–Moynihan (TNMM) model.

The goal of this research is the mathematical description of the temperature field and thermophysical parameters distribution of a glass-metal composite produced by induction heating and the followed cooling based on the TNMM model.

Problem statement

The paper considers the heat transfer and structural transition in production of the engineering glass-and-metal material by the method of inductive heating. The general diagram of the setup and the heated object geometry are shown in Fig. 1. A temperature regime includes the induction heating up to the temperature of glass softening; exposition till the complete press fitting of a glass rod with radius R_1 into a metal cylinder R_2 and their joint cooling; the item annealing with heat-up to the top annealing temperature, then a temperature time exposure, and the cooling with a controlled rate (see a diagram I Fig. 2).

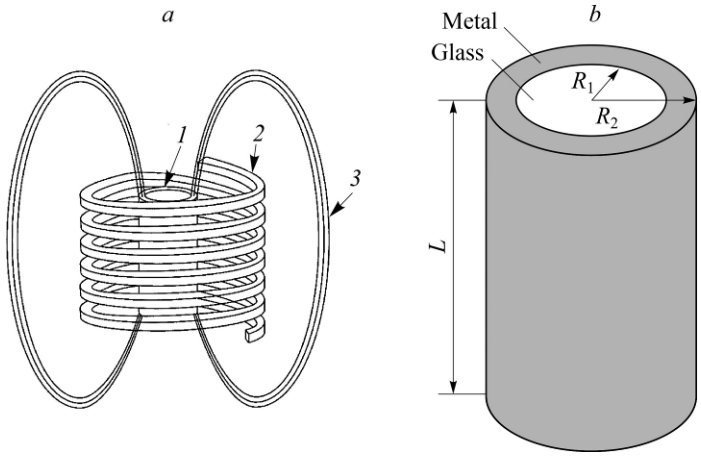

Fig. 1. General diagram of the setup for inductive heating (*a*) and sample geometry (*b*).

a: *1*— heated body, *2* — induction coil, *3* — magnetic field.

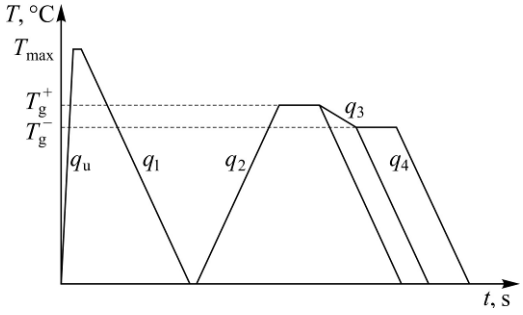

Fig. 2. Temperature regime graph.

The glass heating to the temperature T_{max} (equal or slightly lower than the glass melting temperature T_1) and followed by cooling would change the glass structure and properties. This process is called vitrification and it occurs within a temperature interval with low and high margins $\left(T_g^-, T_g^+\right)$ [4, 5]. The glass transition (vitrification) temperature T_g is in the middle of this interval. The point position depends on the rate of heating-cooling g_1 – g_4 and g_u, and the glass transition margins are typically found from the boundaries of a hysteresis loop (Fig. 3*a*). This loop characterizes, for example, the enthalpy change while uniform heating-cooling cycle from the melt equilibrium state (the curve part denoted as *l*) to the frozen structure (denoted as g).

If we use the TNMM model for description of glass properties within the vitrification interval, the "fictitious temperature T_f" is the key parameter for modeling. For a stabilized state, this temperature T_f becomes equal to the actual temperature ($T_f = T$), while for the frozen structure, we have T_f = const. That is, while uniform-rate cooling, the temperature T_f changes (decreases while cooling) down to the low margin of vitrification interval and then it keeps at a constant level. We also have a concept of "structural temperature". This is used in analysis of experimental data and for differential scanning calorimetry (DSC) in defining the glass transition temperature T_g as a limit for the structural temperature $T_f^* = T_g$. The temperature T_f^* of the "frozen" glass state (see subscript "g" in Fig. 3*a*) is defined as an integral characteristic of

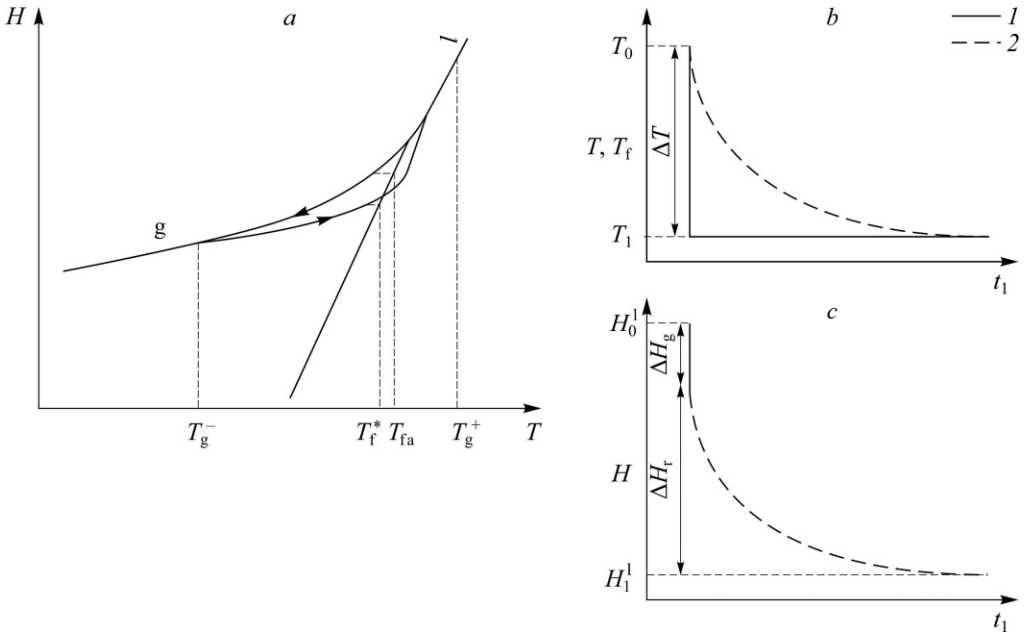

Fig. 3. The temperature dependency for the enthalpy while steady heating and cooling (*a*), equilibrium temperature dependency (*b*) and the change in the enthalpy for the tempearature jump ΔT (*c*).

a: T_g^- and T_g^+ — vitrification range boundaries; *b*: *1* — T °C, *2* — T_f, °C.

a curve for heat capacity c_p:

$$\int_{T^+}^{T_\mathrm{f}^*} \left(c_p^\mathrm{l} - c_p^\mathrm{g}\right) dT_\mathrm{f} = \int_{T^+}^{T^-} \left(c_p - c_p^\mathrm{g}\right) dT, \tag{1}$$

where $T^+ >> T_\mathrm{g}^+$ is the temperature above the vitrification interval, and heat capacity c_p^l takes the equilibrium state value, and T^- is the temperature below the vitrification temperature interval: $T^- << T_\mathrm{g}^-$; c_p^g is the heat capacity of glass in the "frozen" state [4, 5], and we have formulas:

$$\begin{aligned} c_p^\mathrm{g} &= \lim_{\substack{\Delta T\to 0 \\ t-t_1\to 0}} \frac{H - H_0^\mathrm{l}}{\Delta T} = \lim_{\Delta T\to 0} \frac{\Delta H_\mathrm{g}}{\Delta T}, \\ c_p^\mathrm{l} &= \lim_{\substack{\Delta T\to 0 \\ t-t_1\to \infty}} \frac{H - H_0^\mathrm{l}}{\Delta T} = \lim_{\Delta T\to 0} \frac{\Delta H_\mathrm{g} + \Delta H_\mathrm{r}}{\Delta T}, \end{aligned} \tag{2}$$

here ($\Delta H = H - H_0^\mathrm{l}$ is the enthalpy change while the temperature jump $\Delta T = T_0 - T_1$ (Fig. 3*b*). Experimental observations for the glass properties (including enthalpy H) demonstrated that for a temperature jump within the vitrification range, the property changes are classified by two contributions: instant (isostructural) change ΔH_g and relaxational (structural) change ΔH_r) (Fig. 3*c*).

The evolution of the structural temperature can be described by the ratio:

$$\frac{T_\mathrm{f} - T_1}{\Delta T} = \frac{H - H_1^\mathrm{l}}{\Delta H_\mathrm{r}}. \tag{3}$$

Taking into account (1) and (2), we obtain a relatiosnhip used for defining the temperature-dependent glass properties within the vitrification interval:

$$\frac{dT_\mathrm{f}}{dT} = \frac{c_p(T) - c_p^\mathrm{g}(T)}{c_p^\mathrm{l}(T) - c_p^\mathrm{g}(T)}, \tag{4}$$

noting that at $T >> T_\mathrm{g}^+$ $\dfrac{dT_\mathrm{f}}{dT} = 1,$ and for $T << T_\mathrm{g}^-$ $\dfrac{dT_\mathrm{f}}{dT} = 0.$

According to the TNMM model [4, 7, 9–11], the analytical formula for the fictitious tempertaure is the following:

$$T_\mathrm{f} = T_0 + \int_0^t (1 - M_\mathrm{s}(\xi - \dot{\xi})) \frac{dT}{d\dot{\xi}} d\dot{\xi}, \tag{5}$$

where M_s is the function of a structural realaxation of glass properties described through the Kohlrausch function:

$$M_\mathrm{s}(\xi) = e^{-(\xi/\tau_\mathrm{r})^b} = e^{-(\xi K_\mathrm{r}/\eta_\mathrm{r})^b}, \tag{6}$$

where we use the "reduced" time ξ instead of real time t; and the reduced time is related to the real time using a dimensionless function $f(T)$ through the relation $d\xi = f(t)dt$. Typicllay, the reduced time varaiable is defined either through the shear viscosity $\xi(t) = \int_0^t \dfrac{\eta_\mathrm{r}}{\eta(t)} dt$ or thorugh the property relaxation time $\xi(t) = \int_0^t \dfrac{\tau_\mathrm{r}}{\tau(t)} dt,$ where η_r is the reference viscosity

(the shear viscosity at an arbitrary reference temperature (T_r), $\eta(t)$ is the current viscosity, τ_r is the relaxation time at the reference temperature, and $K_\mathrm{r} = \dfrac{\eta_\mathrm{r}}{\tau_\mathrm{r}}$, $0 < b < 1$.

A change in the structural temperture influences the specific heat capacity, viscosity, and the linear thermal expansion coefficient. The specific isobaric heat capacity within the vitrification interval is described (using (4)) in the form:

$$c_p = c_p^\mathrm{g} + (c_p^\mathrm{l} - c_p^\mathrm{g})\frac{dT_\mathrm{f}}{dT}, \tag{7}$$

while the formula for thermal expansion coefficient takes a similar analytical form:

$$\alpha_p = \alpha_\mathrm{g} + (\alpha_\mathrm{l} - \alpha_\mathrm{g})\frac{dT_\mathrm{f}}{dT}. \tag{8}$$

The formula for visocisty as a function of tempertaure and structural changes was adopted from [3] and we render it into a linear relation that links the viscosity logrithm and the value $1/T$:

$$\lg\frac{\eta}{\eta_0} = B_\mathrm{l}\left(T_\mathrm{f}^{-1} - T_0^{-1}\right) + B_\mathrm{g}\left(T^{-1} - T_\mathrm{f}^{-1}\right), \tag{9}$$

here η_0 is the viscosity at temperature T_max, B_l and B_g are the coefficients describing the temperature dependence for η under conditions of equilibrium and frozen structure, correspondingly.

The heat transfer in a conjugate system of a glass-metal composite rod is performed through thermal conductivity mechanism. For the case of a long rod with cylindrical symmetry and thermophysical coefficients depending on temperature-and-material, the thermal conductivity equation is the following:

$$\begin{gathered} c(M,T)\rho(M)\frac{\partial T(M,t)}{\partial t} = \frac{1}{r}\cdot\frac{\partial}{\partial r}\left(\lambda(M,T)r\frac{\partial T(M,t)}{\partial r}\right), \\ t > 0, \quad M \in \Omega = \Omega_1 \bigcup \Omega_2, \\ \Omega_1 = \left\{r : 0 \le r \le R_1\right\}, \ \Omega_2 = \left\{r : R_1 \le r \le R_2\right\}, \end{gathered} \tag{10}$$

where $c(M,T)$, $\rho(M)$, and $\lambda(M,T)$ are the specific heat capacity, material density, and thermal conductivity coefficient (depends on the coordinate and the temperature). The coordinate-dependent thermophysical parameters are written in the form:

$$c, \rho, \lambda = \begin{cases} c_1, \rho_1, \lambda_1, & M \in \Omega_1, \\ c_2, \rho_2, \lambda_2, & M \in \Omega_2. \end{cases} \tag{11}$$

For specific kinds of glass, the glass thermal conductivity λ_1 can have a strong temperature dependence, so we assume $\lambda_1(T)$, while for the metal $\lambda_2 = \mathrm{const}$. For the glass layer in formula (11), the specific heat capacity for the whole temperature range can be described as

$$c_1 = \begin{cases} c_1^{\mathrm{l}}, \ \dfrac{dT_{\mathrm{f}}}{dT} > 1-\delta, \\ c_1^{\mathrm{g}} + \left(c_1^{\mathrm{l}} - c_1^{\mathrm{g}}\right)\dfrac{dT_{\mathrm{f}}}{dT}, \ 1-\delta \le \dfrac{dT_{\mathrm{f}}}{dT} \le \delta, \\ c_1^{\mathrm{g}}, \ \dfrac{dT_{\mathrm{f}}}{dT} < \delta, \end{cases} \tag{12}$$

here δ is a dimensionless parameter depending on the accuracy of measuring derivative $\dfrac{dT_{\mathrm{f}}}{dT}$ and it is assigned independently during the calculations. Here we consider a case of heat transfer in a long cylinder (with axial symmetry), therefore, the temperature at every point M is a function of radius and time only: $T(r, t)$. The boundary conditions are written from the stated assumption in the explicit form: $|T(r, t)| < +\infty$ at $r \to 0$.

The conjunction boundary between materials (glass Ω_1 and metal Ω_2) has a condition of ideal heat contact:

$$T\big|_{r=R_1-0} = T\big|_{r=R_1+0},$$

$$\lambda_1 \frac{\partial T}{\partial r}\bigg|_{r=R_1-0} = \lambda_2 \frac{\partial T}{\partial r}\bigg|_{r=R_1+0}. \tag{13}$$

The temperature regime can be split into two major stages. During the first stage, we consider a process of glass-metal composite fabrication. The second stage is the item annealing for reduction of residual stress (Fig. 2).

However, the first stage comprised three substages: $\mathrm{I_a}$ — the assembled steel cylinder with a glass core is placed into a furnace and heated by the induction heating tool up to the temperature when it becomes soft and welds to the embracing steel cylinder, substage $\mathrm{I_b}$ — exposure at the maximum temperature to ensure the vacuum-sealing contact in the composite, and substage $\mathrm{I_c}$ — cooling of the ready item. Taking all the listed substages, we have the conditions at the outer surface in the form:

$$\lambda_2 \frac{\partial T}{\partial r}\bigg|_{r=R_2} = \nu\left(T - T_{\mathrm{e}}\right) - \sigma\varepsilon\left(T^4 - T_{\mathrm{e}}^4\right) + 10^{-3} \cdot H^2 \cdot \sqrt{\rho\mu f}, \ t \in \mathrm{I_a}, \tag{14}$$

$$T\big|_{r=R_2} = T_{\max}, \ t \in \mathrm{I_b}, \tag{15}$$

$$\lambda_2 \frac{\partial T}{\partial r}\bigg|_{r=R_2} = \nu\left(T - T_{\mathrm{e}}\right) - \sigma\varepsilon\left(T^4 - T_{\mathrm{e}}^4\right), \ t \in \mathrm{I_c}, \tag{16}$$

where ν is the thermal conductivity coefficient, T_{e} is the ambient temperature, σ is the Boltzmann constant, ε is the emission coefficient, H is the magnetic field amplitude, ρ is the electromagnetic resistance for the heated body, μ is the magnetic permeability coefficient, and f is the electromagnetic field frequency for induction tool.

The second stage is the product annealing. The annealing has to remove the internal stress caused by irregular cooling of glass. The limits for annealing procedure are assigned by the viscosity values 10^{12}– $10^{13.5}$ Pa·s. The top limit for annealing temperature is the top annealing temperature $T_{\mathrm{ann}}^{\mathrm{top}}$ (which corresponds to the glass viscosity at the level of 10^{12} Pa·s), the three-minute exposure at this temperature kills about 95 % of internal stress and does not induce the item deformations. The second characteristic temperature for annealing procedure is $T_{\mathrm{ann}}^{\mathrm{low}}$ (lower than $T_{\mathrm{ann}}^{\mathrm{top}}$ by 50–150 °C). The three-minute exposure at $T_{\mathrm{ann}}^{\mathrm{low}}$ removes only 5 %

of internal stress. The cooling rate in the temperature range [$T_{\text{ann}}^{\text{low}}$, $T_{\text{ann}}^{\text{top}}$] should be minimal, and outside this interval, it can be any.

The process of annealing can be arranged in alternative ways: the controlled cooling on the stage I_c or the second heating followed by cooling cycle divided into three substages — II_a, II_b, and II_c. The second heat-up can be performed by induction heating (induction furnace) with later removal of the sample into a muffle furnace for the rate-controlled cooled. The stage II_a is the sample cooling from the maximum temperature ($T_{\max}$) to the top annealing temperature $T_{\text{ann}}^{\text{top}}$ with an arbitrary rate, the stage II_b is the cooling from $T_{\text{ann}}^{\text{top}}$ with a controlled rate to the low annealing temperature $T_{\text{ann}}^{\text{low}}$, and the next stage II_c is the cooling from $T_{\text{ann}}^{\text{low}}$ to the room temperature at any rate. The boundary conditions for the outer surface of the metal cylinder are the following:

$$t \in \text{II}_{\text{a,b,c}} \lambda_2 \left.\frac{\partial T}{\partial r}\right|_{r=R_2} = \nu\left(T - T_{\text{e}}^{\text{a,b,c}}\right) - \sigma\varepsilon\left(T^4 - T_{\text{e}}^4\right), \tag{17}$$

here $T_{\text{e}}^{\text{a,b,c}}$ is the temperature of medium satisfying the a-b-c conditions $\dfrac{\partial T_{\text{e}}^{\text{a}}}{\partial t} = q_{\text{a}}$, $\dfrac{\partial T_{\text{e}}^{\text{b}}}{\partial t} = q_{\text{b}}$, and $\dfrac{\partial T_{\text{e}}^{\text{c}}}{\partial t} = q_{\text{c}}$.

The boundary conditions (14)–(17) on the free surfaces indicate that the heat is drained only through the outer surface of the item. The stated problem is significantly nonlinear, so it could be resolved in approximations.

Numerical method and algorithm of solution

The boundary-value problems for nonlinear parabolic equations can be solved approximately. One of the most universal and efficient methods is the finite difference method. For the area $\Omega = \left(0 \le r \le R_2,\ 0 \le t \le T\right)$ we construct a rectangular mesh $\overline{\omega} = \overline{\omega}_1 \times \overline{\omega}_2$:

$$\overline{\omega}_1 = \left\{ r_i = i\Delta r,\ i = 0,\ 1,...,\ I_1,...,I,\ r(0) = 0,\ \sum_{i=1}^{I_1} \Delta r = R_1,\ \sum_{i=I_1}^{I} \Delta r = R_2 \right\},$$

$$\overline{\omega}_2 = \left\{ t_n = n\Delta t_n,\ n = 0,\ 1,...,N,\ \sum_{n=1}^{N} \Delta t_n = t_{\text{end}} \right\}.$$

We introduce a mesh function $T_i^{\,n} = T\left(r_i,\, t_n\right)$ on the mesh $\overline{\omega}$. The numerical solution of nonlinear equations (10) can be easily performed through implicit schemes; they are stable and monotonic at any choice of steps [14]. There exist two major variants of those difference schemes. For the first (linear) implementation, the coefficients λ and c on (n + 1) time layer depend on the temperature of the previous layer (n). The scheme reduces to the solution of a linear equation system with a three-diagonal matrix and the diagonal prevalence of elements. For the second (nonlinear) scheme, the coefficients λ and c depend on the temperature on the current (n + 1) layer, so the scheme becomes nonlinear and is solved numerically by iteration methods, e.g., by sequential approximation method. Note here that for a single iteration only, this method coincides with the linear method. With a trend for considering the vitrification interval in this paper, we consider the linear variant, so equation (10) takes the form:

$$\frac{1}{i\Delta r^2}\left(\left(i+\frac{1}{2}\right)\lambda^n_{i+\frac{1}{2}}\left(T^{n+1}_{i+1}+T^{n+1}_i\right)-\left(i-\frac{1}{2}\right)\lambda^n_{i-\frac{1}{2}}\left(T^{n+1}_i-T^{n+1}_{i-1}\right)\right)=c^n_i\rho_i\frac{T^{n+1}_i-T^n_i}{\Delta t_n}, \quad (18)$$

$$\lambda^n_{i+\frac{1}{2}}=\frac{1}{2}\left(\lambda^n_i+\lambda^n_{i+1}\right), \quad \lambda^n_{i-\frac{1}{2}}=\frac{1}{2}\left(\lambda^n_i+\lambda^n_{i-1}\right), \quad \lambda^n_i=\lambda^n_i\left(T^n_i\right), \quad n=1,...,N.$$

This scheme is A-stable, conservative, monotonic, and has the approximation error $O\left(\Delta t+\Delta r^2\right)$.

The specific heat capacity in equations (18) satisfies condition (7) and its approximations for steps $i = 0, 1, ..., I_1$ at $k = 1$ take the form:

$$c^n_i=\begin{cases} c^l, \ \dfrac{T^n_{\mathrm{f}i}-T^{n-1}_{\mathrm{f}i}}{T^n_i-T^{n-1}_i}>1-\delta, \\ c^{\mathrm{g}}+\left(c^{\mathrm{l}}-c^{\mathrm{g}}\right)\dfrac{T^n_{\mathrm{f}i}-T^{n-1}_{\mathrm{f}i}}{T^n_i-T^{n-1}_i}, \ 1-\delta\le\dfrac{T^n_{\mathrm{f}i}-T^{n-1}_{\mathrm{f}i}}{T^n_i-T^{n-1}_i}\le\delta, \\ c^{\mathrm{g}}, \ \dfrac{T^n_{\mathrm{f}i}-T^{n-1}_{\mathrm{f}i}}{T^n_i-T^{n-1}_i}\le\delta. \end{cases} \quad (19)$$

For finding the specific heat capacity, we can approximate the fictitious temperature. Application of the superposition principle to the description of structural relaxation (5) can be presented in the following manner. The description of temperature fields at every point of glass-forming zone can be taken as a set of constant values T^n_i on short time intervals Δt. In transition from $(n-1)$th interval on the nth interval, we have a temperature jump ΔT^n_i and the actual temperature T^n_i changes instantly. Meanwhile, temperature $T^n_{\mathrm{f}i}$ cannot change instantly, so there is a difference between the structural and the actual temperature $\Delta T^n_{\mathrm{f}i}=T^n_{\mathrm{f}i}-T^n_i$, and this difference relaxes down in the next time intervals, therefore, the value $T^n_{\mathrm{f}i}$ equals the initial value of structural temperature and the sum of all relaxation processes from the initial to final time. Relaxation of structure brings a change in properties (7)–(9), including the viscosity (again influencing the structure relaxation). It is approximated by a linear scheme and the rectangular formula for calculation of integral (7) (by analogy with specific heat capacity and thermal conductivity coefficient). The value of viscosity is taken from the previous nth time layer; then we calculate the structural temperature, then the viscosity, and later the rate of relaxation processes at the $(n+1)$th layer:

$$T^{n+1}_{\mathrm{f}i}=T^{n+1}_{\max}+\sum_{m=1}^{n+1}\left(1-e^{-\left(\frac{K_{\mathrm{r}}}{\eta_{\mathrm{r}}}\left(\xi^{n+1}_i-\xi^{m-1}_i\right)\right)^b}\right)\left(T^m_i-T^{m-1}_i\right),$$

$$\xi^{n+1}_i=\sum_{m=1}^{n+1}\frac{\eta_{\mathrm{r}}}{\eta^{m-1}_i}\Delta t_m, \quad (20)$$

$$\lg\frac{\eta^{n+1}_{ji}}{\eta_r}=B_{\mathrm{l}}\left(\frac{1}{T^{n+1}_{\mathrm{f}i}}-\frac{1}{T^0_{\max}}\right)+B_{\mathrm{g}}\left(\frac{1}{T^{n+1}_i}-\frac{1}{T^{n+1}_{\mathrm{f}i}}\right), \ n=0,...,N,$$

here $T_{\max}^0$ is the initial condition for calculation of the fictitious temperature after the inductive heating. The boundary conditions are approximated with account for preserving the approximation error $O\left(\Delta t + \Delta r^2\right)$ by standard methods used in the theory of differential schemes [14]. Here we take the constant boundary conditions at $r = 0$ and at $r = R_1$:

$$i = 0: \frac{T_0^{n+1} - T_0^n}{\Delta t_n} = \frac{4}{\Delta r^2} \lambda_{1/2}^n \left(T_1^{n+1} - T_0^{n+1}\right), \quad \lambda_{1/2}^n = \frac{\lambda_0^n + \lambda_1^n}{2}, \tag{21}$$

$$i = I_1: \frac{\lambda_{I_1-1/2}^n}{\Delta r}\left(T_{I_1}^{n+1} - T_{I_1-1}^{n+1}\right)\left(1 - \frac{1}{I_1}\right) + \frac{c_{1I_1}^n \rho_1 \Delta r}{\Delta t_n}\left(T_{I_1-1}^{n+1} - T_{I_1-1}^n\right) =$$

$$= \frac{\lambda_{I_1+1/2}^n}{\Delta r}\left(T_{I_1+1}^{n+1} - T_{I_1}^{n+1}\right)\left(1 + \frac{1}{I_1}\right) - \frac{c_2 \rho_2 \Delta r}{\Delta t_n}\left(T_{I_1+1}^{n+1} - T_{I_1+1}^n\right), \tag{22}$$

$$\lambda_{I_1+1/2}^n = \frac{\lambda_{2I_1}^n + \lambda_{I_1+1}^n}{2}, \quad \lambda_{I_1-1/2}^n = \frac{\lambda_{1I_1}^n + \lambda_{I_1-1}^n}{2}.$$

The outer boundary conditions (at $r = R_2$) are different for different stages — vary from (14) to (17). Here we present the digital approximation for the most complex condition (14) that models the induction heating $\left(t \in I_{\text{a}}\right)$:

$$\frac{\lambda_{I-1/2}^n}{\Delta r}\left(T_I^{n+1} - T_{I-1}^{n+1}\right)\left(1 - 1/I\right) + \frac{c_2 \rho_2 \Delta r}{\Delta t_n}\left(T_{I-1}^{n+1} - T_{I-1}^n\right) =$$

$$= \theta\left(T_I^{n+1} - T_{\text{e}}\right) - \sigma\varepsilon\left(\left(T_I^{n+1}\right)^4 - T_{\text{e}}^4\right) + 10^{-3} H^2 \sqrt{\rho \mu f}, \tag{23}$$

$$\lambda_{I-1/2}^n = \frac{\lambda_{2I}^n + \lambda_{2I+1}^n}{2}.$$

The other conditions are approximated similarly.

The algorithm of solving the system (13), (18), and (22) is closed by the boundary conditions (15) or (17) and is reduced to solving a set of linear algebraic equations with the Thomas method, while the structural changes on every time level are calculated from equations (17) and (18). The boundary conditions at the external (metal) surface (14) and (16) are nonlinear, therefore, we have to solve the system (18)–(22) under boundary conditions (14) or (16) by the sweep method, but now this method was slightly modified: it takes only one nonlinear equation at the *I*th step. Actually, the system comprises *I* linear equations with a three-diagonal matrix and one nonlinear equation (for unknowns from the $(I - 1)$th and *I*th step. Thus, this method offers the formulation for unknowns from the previous step. In this way, the last nonlinear equation has only one unknown variable T_1^{n+1} and this is a fourth-order equation with real coefficients. The general form of this equation is the following:

$$AX^4 + BX + C = 0, \quad X = T_I^{n+1},$$

and this equation admits analytical form of roots; three of roots are irrelevant (they are a pair of conjugate complex numbers and one is a real negative number. Thus, we obtain a single relevant analytical solution. By inserting this solution into the standard formulas for sweep method, we obtain all unknowns for the system. However, this algorithm cannot be applied for the problem of heat transfer in a cylindrical layer with nonlinear conditions of type (14) or (15) for the external surface of the inner radius. For this case, the problem with a set of nonlinear equations can be solved by numerical iteration methods.

Numerical simulation results

In all simulations, we used the data accumulated in Table 1 and the treatment regimes shown in Table 2, along with additional parameters: $T_{max} = 760$ °C, $R_1 = 4 \cdot 10^{-3}$ m, $R_2 = 5 \cdot 10^{-3}$ m, $f = 50$ Hz, $\sigma = 5.670367 \cdot 10^{-8}$ W·m^{-2}·K^{-4}, and $H = 4 \cdot 10^4$ A/m. Simulations demonstrated that at the start of cooling process, the structural temperature equals the actual temperature, but later it delays in cooling stage and tends to a constant value. Similarly, during the heating process, it deviates from a constant value, but later coincides with the varying actual temperature. This behavior repeats for heating/cooling cycles (Fig. 4). The detailed behavior of fictitious temperature is plotted in the dedicated graphs below the main curve (these fragments are marked by squares allocated from left to right). This characteristic change in the fictitious temperature is instrumental in defining the vitrification temperature limits; these are the temperatures when the rate of fictitious temperature vs. temperature (Fig. 5*a*) is different from 0 or 1. Correspondingly, this means a difference from the frozen-state-glass and from the equilibrium melt. This state would change the values of specific heat capacity (7), linear coefficient of thermal expansion (8), and viscosity (9) (Figs. 5*b*–5*d*). These curves are in compliance with the relaxation theory of vitrification. Paper [5] offered a thermodynamic justification for deviating of the specific heat capacity from the stable (frozen) and equilibrium states (see dashed areas in Fig. 6): this is a result of internal exothermic (Fig. 6*a*) and endothermic (Fig. 6*b*) processes. The after-cooling repeated heating releases a part of excessive heat that has been frozen in glass due to relaxation processes, thus, it needs a lower amount of heat for temperature growth in the interval approximately

Table 1

Thermophysical coefficients and approximation parameters [4, 15]

Material property	Glass C52-1	Steel C20
c_1^l, J/(kg·°C)	2950	477
c_1^g, J/(kg·°C)	820	
Λ, W/(m·°C)	$\lambda = (0.81 + 0.213 \cdot 10^{-2} T - 1.02 \cdot 10^{-6} T2)$	$\lambda = (29 - 0.03T)$
ρ_1, kg/m^3	2300	7876
B_1, °C	18763	–
B_g °C	13763	–
$\alpha_l \cdot 10^{-5}$, °C^{-1}	210	152
α_g, °C^{-1}	52	121
lg η_r	10.25	–
lg K_r	10.7	–
b	0.65	0.65
μ	–	100
ρ, Ω·m	–	$16.9 \cdot 10^8$
ε	–	0.55

Table 2

The temperature change rate $q = \dfrac{\partial T}{\partial t}$ for operational stages as shown in Fig. 2

Regime #	q_u, °C/min	q_1, °C/min	q_2, °C/min	q_3, °C/min	q_4, °C/min
1	90	10	90	1.5	1.5
2				3	3
3			10	1.5	1.5
4				3	3
5		3	3	3	3

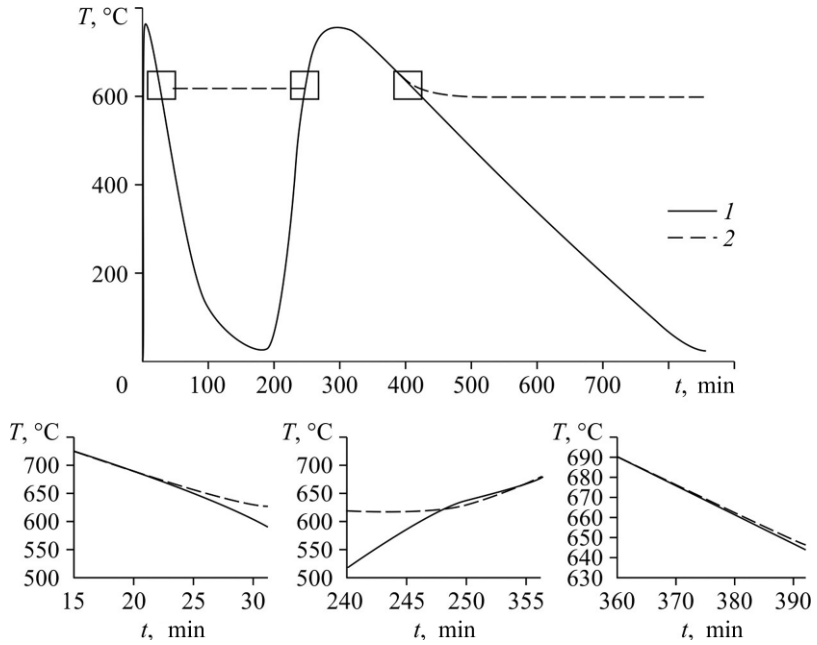

Fig. 4. Glass temperature evolution at $r = R_1$ by Regime 3 (Table 2).
1 — $T(t)$, *2* — $T_f(t)$.

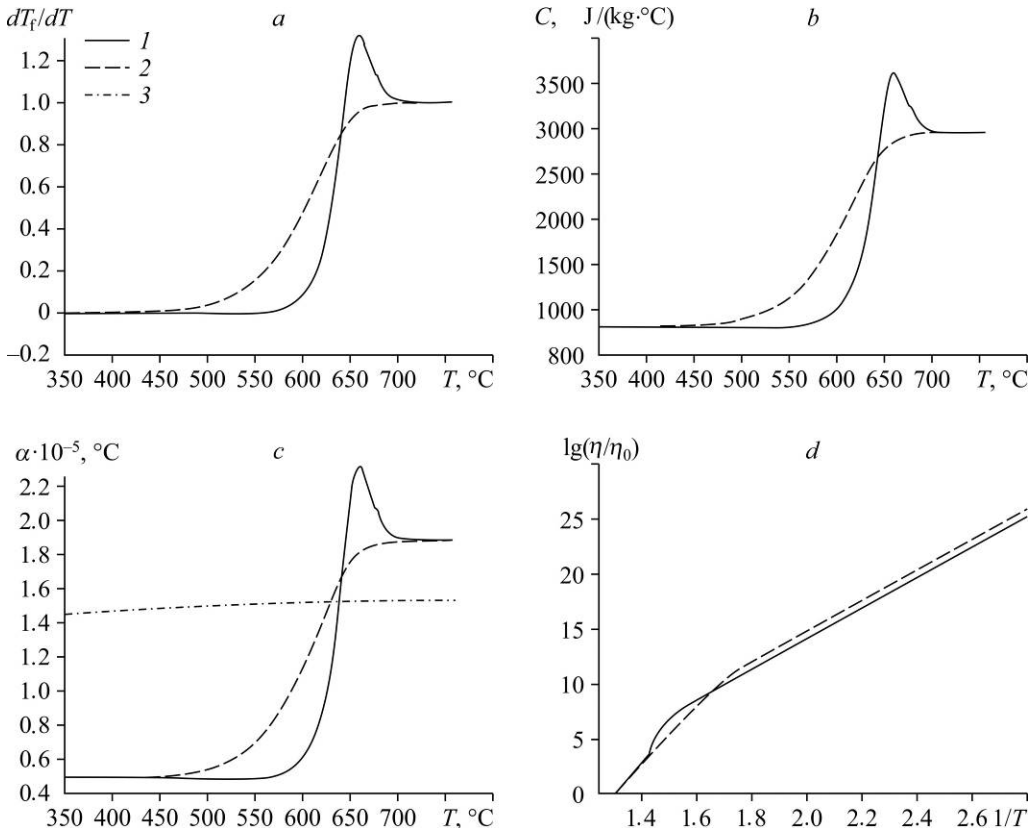

Fig. 5. Temperature dependences for: change on fictitious temperature (*a*), specific heat capacity (*b*), linear thermal expansion coefficient (*c*), and viscosity during annealing (*d*) by regime 3 from Table 2 at $r = R_1$.
1 — heating , *2* — cooling, *3* — linear thermal expansion coefficient for steel.

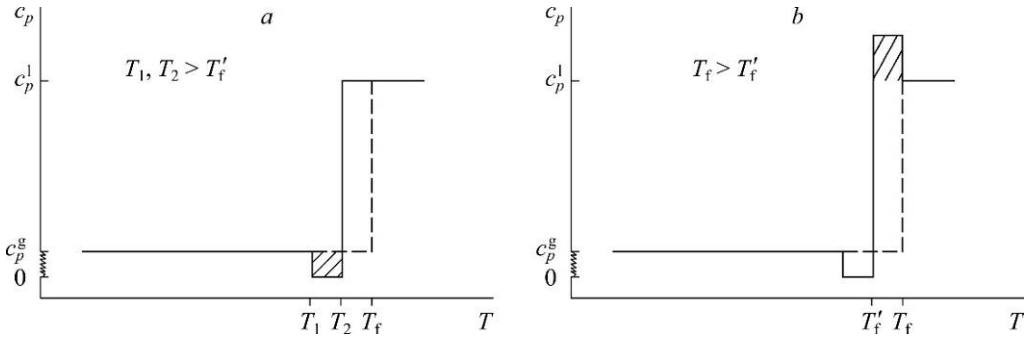

Fig. 6. Contributions to the effective heat capacity while glass heating [5].
Exothermic (*a*) and endothermic (*b*) processes.

from T_1 and T_2, so the heat capacity becomes lower than c_p^g, while the value of fictitious temperature for the new state shifts to $T_f' < T_f$. With the temperature growth, the system increases its thermal storage, and the thermodynamic functions become as for an equilibrium liquid before the frozen structure (or primary glass) at the fictitious temperature T_f, therefore, the current heat capacity becomes higher than c_p^g.

In experimental production of a glass-metal composite rod through induction heating, we noted a faster cooling of samples as compared to the simulation results. The discrepancy between experiment and simulation was removed through accounting of thermal radiation from the outer metal cylinder. The curves in Fig. 7 demonstrate the difference in simulations under boundary conditions (14)–(17) with/without radiation contribution.

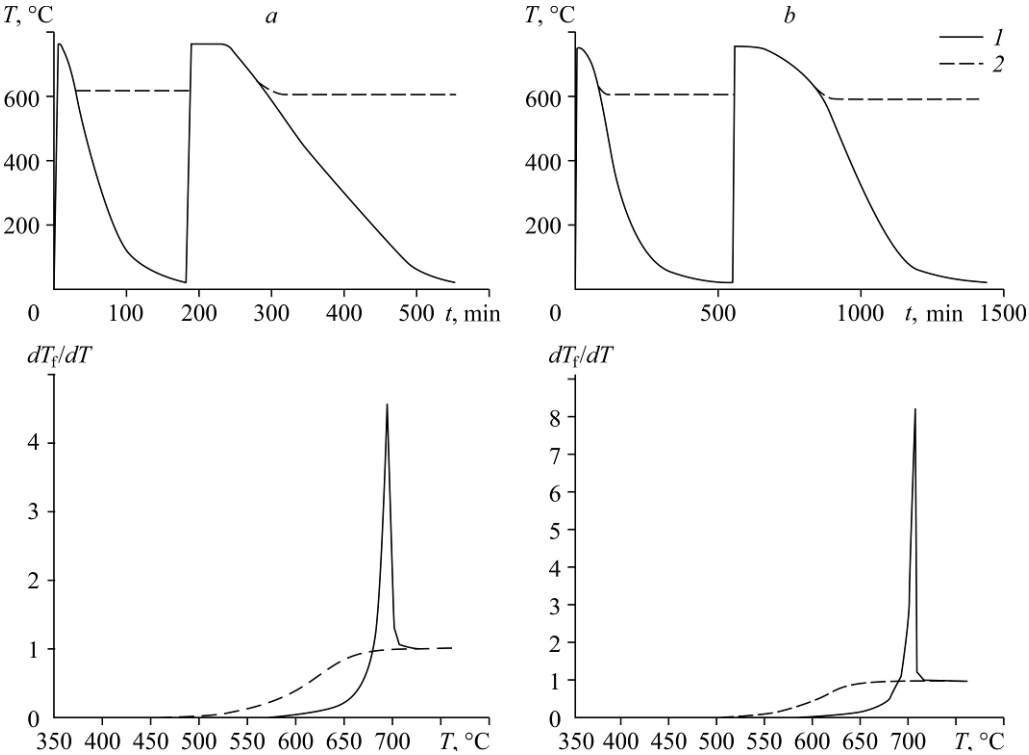

Fig. 7. Temperature distribution at $r = R_1$ according to Regime 1 from Table 2
with (*a*) and without (*b*) radiation contribution.
1 — $T(t)$, *2* — $T_f(t)$.

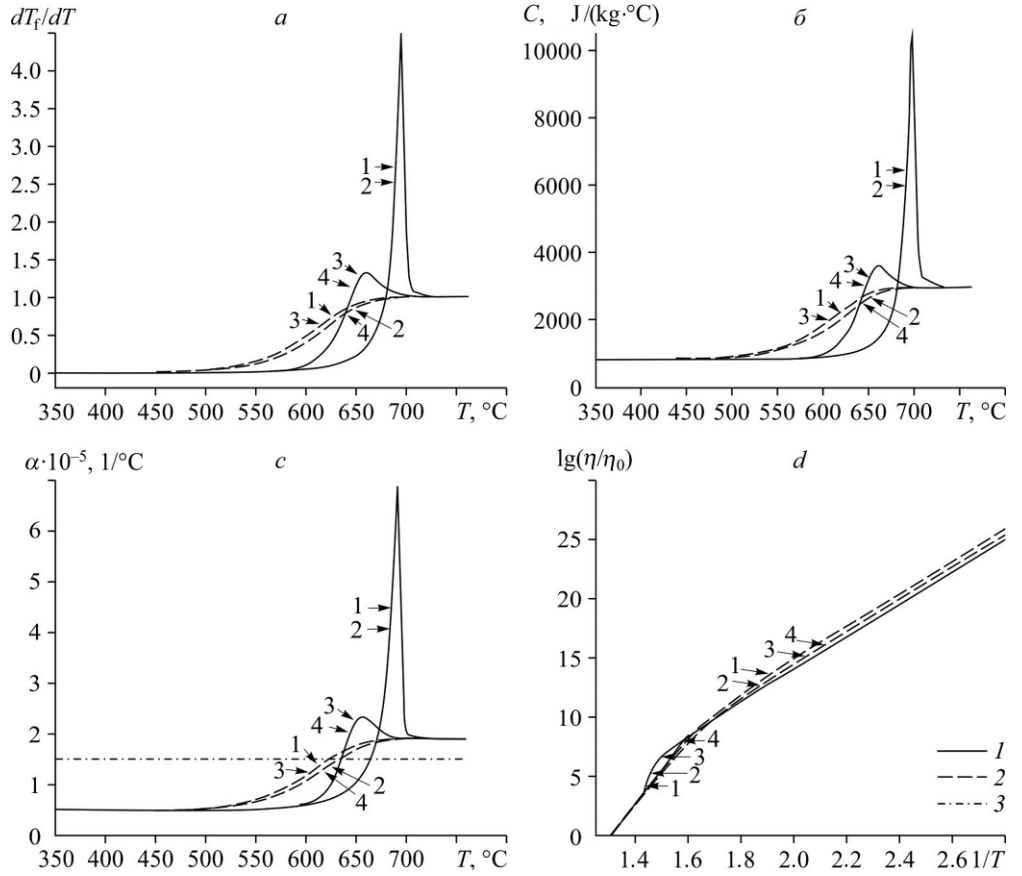

Fig. 8. Temperature dependencies for parameters: fictitious temperature (*a*), specific heat capacity (*b*), linear thermal expansion coefficient (*c*), viscosity (*d*) during annelaing for modes 1-4 (Table 2) at $r = R_1$.
1 — heating, *2* — cooling,
3 — variation of the linear thermal expansion coefficient for steel.

Analysis of evolution in thermophysical properties for different modes of annealing (Fig. 8) revealed that for a higher heating rate, the top temperature of annealing (here the top margin of vitrification interval) shifts to higher values. For the given pair of materials, this is about 700–750 °C, meanwhile the heating at a lower rate gives the top temperature of annealing about 650–700 °C. The calculated curves for the linear thermal expansion coefficient at a high temperature rate (for the vitrification interval) demonstrate a rapid increase: the top value of this coefficient is by 5 times bigger than the linear coefficient. Note as well that the low annealing temperature (the low limit for vitrification range) for all tested regimes is almost the same and belongs to the interval (480, 530)°C.

Figures 5 and 8*c* depict a special temperature where the curves for linear temperature expansion for glass and metal while heating/cooling have an intersection point. At this temperature, the mechanical stress in the glass-metal seal changes its sign. For the case of planar seals, operator can choose a cooling mode that the cooling-induced stress can be reduced through the increase in compressing stress. Therefore, the rate of temperature decline is taken at a low level for the temperature range between the top annealing temperature and the crossing point for graphs of linear thermal expansion for glass and metal (Figs. 9–11).

The evolution of temperature and properties of the sample on the glass rod diameter (keeping the same ratio of the metal shield to the glass core) demonstrates that if the glass diameter is lower than $2 \cdot 10^{-2}$ m, the temperature drop over the radius is less than 2 °C (Fig. 9).

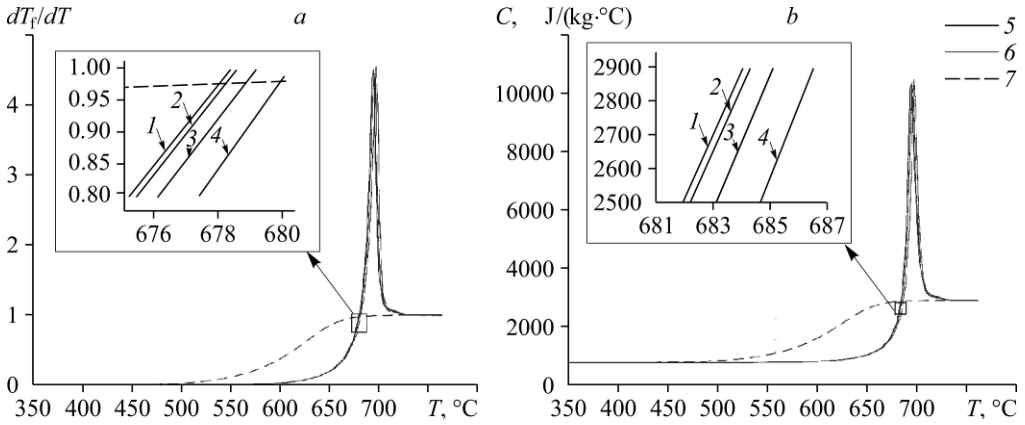

Fig. 9. Temperature dependencies for parameters: fictitious temperature (*a*) and specific heat capacity at annealing (*b*) by regime 1 from Table 2.
$r = 0$ m (*1*), 0.0013 m (*2*), 0.0027 m (*3*), and 0.0040 m (*4*); *5* — heating, *6* — cooling, *7* — evolution of linear thermal expansion coefficient (steel).

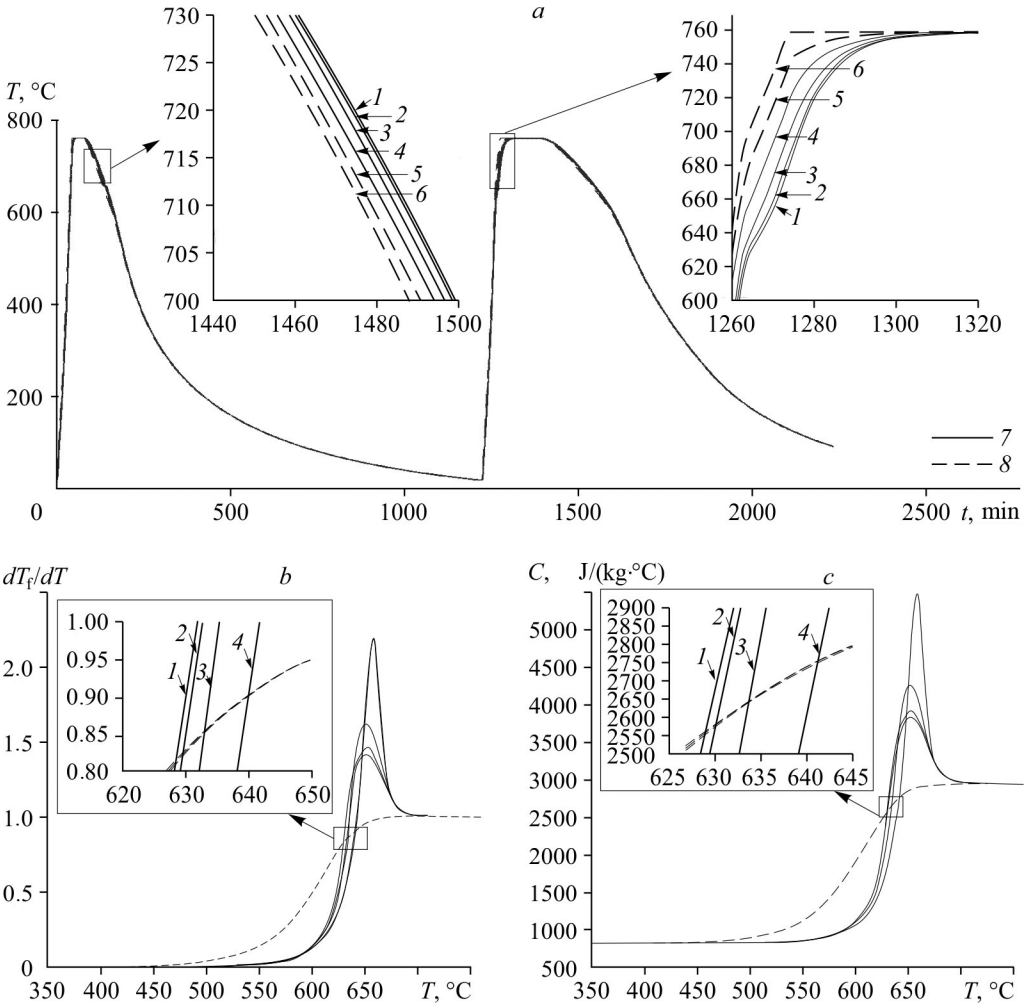

Fig. 10. Change in tempertaure for different radial points (*a*), change in fictitious temperature (*b*) and specific heat capacity (*c*) at annealing for $R_1 = 4 \cdot 10^{-2}$ m and $R_2 = 5 \cdot 10^{-2}$ m (regime #1 from Table 2).
For the center of a glass cylinder (*1*), $r = 1.3 \cdot 10^{-2}$ m (*2*), $2.7 \cdot 10^{-2}$ m (*3*), $4 \cdot 10^{-2}$ m (*4*), $4.5 \cdot 10^{-2}$ m (*5*), $5 \cdot 10^{-2}$ m (*6*); *a*: glass (*7*), steel (*8*), *b*, *c*: heating (*7*), cooling (*8*).

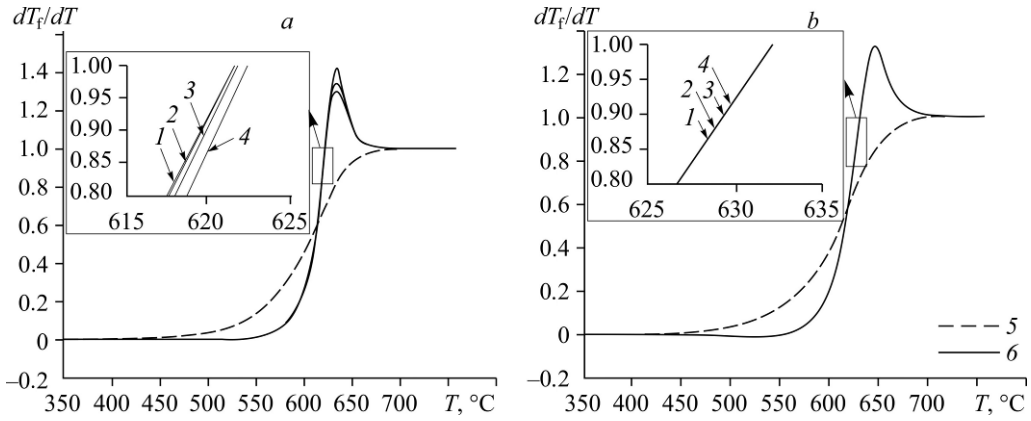

Fig. 11. Rate of change in the fictitious temperature while annealing.

a — $R_1 = 4\cdot10^{-2}$ m and $R_2 = 5\cdot10^{-2}$ m by regime 5 from Table 2: *1* — at the glass cylinder center, $r = 1.3\cdot10^{-2}$ m (*2*), $2.7\cdot10^{-2}$ m (*3*), $4\cdot10^{-2}$ m (*4*); *5* — heating, *6* — cooling; *b* — $R_1 = 4\cdot10^{-3}$ m and $R_2 = 5\cdot10^{-3}$ m by regime from Table 2. At the glass cylinder center (*1*), $r = 1.3\cdot10^{-3}$ m (*2*), $2.7\cdot10^{-3}$ m (*3*), $4\cdot10^{-3}$ m (*4*); *5* — heating, *6* — cooling.

Obviously, all of simulated properties are very close for all radial points. As the diameter of the glass rod increases up to $5\cdot10^{-2}$ m, a temperature distribution over the radius is observed. This can be significant during sample heating: this temperature difference is up to 20 °C. For the cooling regime, this radial difference in the glass core becomes lower than 5 °C, and this can be found in tracking of tested sample properties (Fig. 10).

The validation of the solved numerical problem (1)–(17) was conducted through a series of experiments measuring of shrinkage shift after heating a glass rod. Experiments were performed by the method developed in [16] for glass cylinders (with the diameter of 8 mm with a controlled heating rate 10 °C/min); a special lab setup similar to a load-type viscometer was constructed. It was shown in [16] that the shrinkage displacements for glass rod have the *S*-shaped profile, and the temperature range for this profile is close to the vitrification range. Comparison of experimental data with calculated values for the linear thermal expansion coefficient (regime #4 in Table 2) is shown in Fig. 12. Note that the experimental data on shrinkage effect give a good qualitative description. Therefore, the idea of finding the vitrification interval from the measuring of glass rod shrinkage is quite justified.

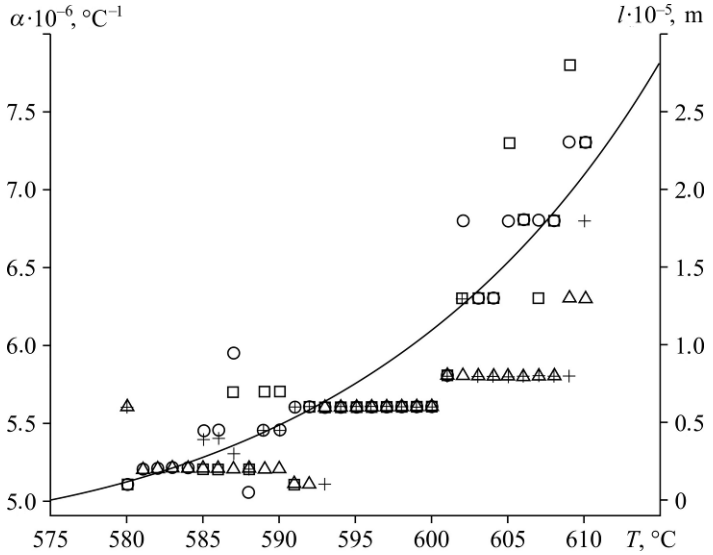

Fig. 12. Experimental results for shrinkage effect (symbols) and data from numerical approximation for the coefficient (curve) for regime #4 from Table 2.

Conclusion

The problem of complex heat transfer for a two-layered glass-metal cylindrical composite was stated and solved for the entire technology interval of production and the follow-up annealing (with account for vitrification process). Numerical simulation of vitrification process was performed in the framework of the relaxation theory and the TNMM model. A solving algorithm for the stated problem has been developed. Simulation was applied to different regimes of annealing, including the induction heating variant For the case of induction heating, a linear thermal expansion coefficient exhibits a rapid growth within the vitrification interval; it becomes three times higher than for a slow-rate regime. Besides, this value exceeds the linear thermal expansion coefficient for the steel shield, and this would create the growth of stress at heating during the annealing stage (in both glass and metal layer).

References

1. **V.V. Pikul,** Efficiency of glass-metal composites, Perspektivnye Materialy, 2000, No. 6, P. 63–65.
2. **L.S. Zimin and A.V. Baikin,** Using of inductive heating in industrial technologies, State of art and perspectives in electric technologies, in: Proc. Scientific Conf. (XVII Beradanos' Lections). Vo. 1, Ivanovo, 2013, P. 3–7.
3. **O.V. Mazurin,** Annealing for Glass-to-metal Seal, Energia, Leningrad, 1980.
4. **O.V. Mazurin,** Glass Transition, Nauka, Leningrad, 1986.
5. **S.V. Nemilov,** Optical Material Science: Thermodynamic and Relaxation Properties of Glass-Producing Melts and Glasses, St.Peterburg: SPSU ITMO, 2014.
6. **Yu.K. Startsev,** Relaxation Phenomena in Glasses for Vitrification While Annealing, Glass-Salt Melt Ion Exchange and in Seals; Ph.D diss, , 01.04.07. St. Petersburg, 2001.
7. **T.V. Tropin, J.W.P. Schmelzer, and V.L. Aksenov,** Modern aspects of the kinetic theory of glass transition, Physics-Uspekhi, 2016, Vol. 186, No. 1, P. 42–68.
8. **C.T. Moynihan, P.B. Macedo, C.J. Montrose, P.K. Gupta, M.A. DeBolt et al.** Structural relaxation in vitreous material, Ann. N. Y. Acad. Sci.,1976, Vol. 279, P. 15–35.
9. **O.S. Narayanaswami,** A model of structural relaxation in glass, J. Amer. Ceram. Soc., 1971, Vol. 54, No. 10, P. 491–498.
10. **J.W.P. Schmelzer,** Kinetic criteria of glass formation and the pressure dependence of the glass transition temperature, The J. Chemical Phys., 2012, Vol. 136, No. 7, P. 074512-1–074512-11.
11. **A.Q. Tool,** Relation between inelastic deformability and thermal expansion of glass in its annealing range, J. Amer. Ceram. Soc., 1946, Vol. 29, No. 9, P. 240–253.
12. **N.A. Rubtsov,** To analysis of heating and melting processes in a layer of semitransparent material, Thermophysics and Aeromechanics, 2012, Vol. 19, No. 4, P. 629–640.
13. **N.A. Rubtsov and S.D. Sleptsov,** Radiant-conductive heat transfer in semitransparent medium with phase transition at boundaries with different absorptivity, Thermophysics and Aeromechanics, 2010, Vol. 17, No. 2, P. 221–228.
14. **A.Yu. Krainov and L.L. Minkov,** Numerical Methods for Solving Heat and Mass Transfer Problems; Student training material, STT, Tomsk, 2016.
15. **S.A. Chernavskii and V.F. Reschikov,** Metal Engineer Handbook, Vol. 1, 3rd edition, Mashinostroenie, Moscow, 1976.
16. **O.N. Lyubimova and S.A. Dryuk,** Simulation parameters of temperature in the process of manufacturing a glass-metal composite, Thermophysics and Aeromechanics, 2017, Vol. 24, No. 1, P. 127–135.